Novel continuously tunable high spectral resolution optical filter for two-dimensional imaging

Pritish Mukherjee,[a] Shudong Chen,[b] and Sarath Witanachchi
Laboratory for Advanced Materials Science and Technology (LAMSAT), Department of Physics, University of South Florida, Tampa, Florida 33620

(Received 16 October 2000; accepted for publication 6 March 2001)

Despite the existence of a variety of optical filters for the separation of spectral components in a multicolor image, a filter that is both continuously wavelength tunable and capable of high spectral resolution while preserving the spatial integrity of a two-dimensional image is not currently available. We present, in this article, the introduction of a novel optical filtering concept that permits the development of such a system. Both the concept and its implementation in an optical-fiber-based prototype that converts two-dimensional images to a one-dimensional array followed by interconversion for image reconstruction are presented. The performance of the prototype is analyzed using both a xenon arc lamp as a standard broadband illumination source as well as He–Ne and Ar lasers as sources of coherent radiation. An unoptimized throughput efficiency of approximately 30% and a bandwidth of 6 Å without spectral leakage or spatial crosstalk is obtained over the entire investigated tuning range from 430 to 807 nm. Potential applications of such an optical filtration system, with wavelength tunability on the angstrom scale and potential spatial resolutions in the micrometer range, using suitable optical imaging are discussed. © *2001 American Institute of Physics.* [DOI: 10.1063/1.1370562]

I. INTRODUCTION

The spectral filtering of a multicolor image has been widely studied.[1] These studies have resulted in filters that employ absorption,[2–7] dispersion,[7–11] selective reflection,[12–15] or spectrally selective transmission.[1,16–22] Based on these general concepts, a variety of techniques are currently available for spectral image filtering.[1,23] These include, among others, dichroic coated filters,[24–27] holographic filters,[28–35] acousto-optic tunable filters,[35] Fabry–Perot tunable filters,[24,35–39] tunable birefringent filters,[23,40–46] and Lyot filters.[23,47–49] The filtration mechanisms vary from the use of Bragg diffraction caused by periodically modulated refractive indices in holographic and acousto-optic tunable filters, to the use of selectivity in transmission by polarization in Lyot filters. The basic underlying objective is the absorption, transmission, or reflection of a selected spectral range. These techniques and their development to enhance the tunability and spectral sensitivity have been ongoing for several decades.[50–52] Fiber spectroscopic systems using linear fiber arrays are in use in both the Optical Spectroscopic system at the UK Schmidt telescope and the Sloan Digital Sky Survey system.

High sensitivity charge-coupled-device (CCD) cameras can be combined with notch filters for high spectral resolution two-dimensional imaging, or with band pass filters for broadband imaging. However, the dual requirements of fidelity of two-dimensional spatial imaging and high resolution continuous spectral tunability are not available in such currently existing systems. We present, in this article, a new concept of optical filtering suitable for this purpose and describe its implementation in a laboratory prototype. This system is especially useful to study two-dimensional images at any desired wavelength. The optical arrangement that allows the implementation of this spectral filter and its fabrication and characterization are discussed in detail. The performance of the system is analyzed using both standard broadband illumination and coherent laser sources.

II. NEW CONCEPT OF TWO-DIMENSIONAL, TUNABLE SPECTRAL FILTERING

The basic objective is to fabricate an optical filter that will separate an incident multifrequency two-dimensional image into spectral components while retaining the integrity of the two-dimensional image. When a two-dimensional image is incident on a diffraction grating, each point on the image is angularly separated in different directions according to the spectral content of the image. The output of the grating, i.e., the angularly separated image, will result in an overlap of both spectral and spatial components of the image which makes it impossible to obtain any useful information. The key to a solution for this problem is to use suitably arranged optical fiber bundles to maintain image integrity while accurately redirecting the spectral components after separation. By suitably arranging the fiber array, the image can be angularly and spatially separated without overlap, so that it is possible to obtain the two-dimensional image at any desired wavelength.

The concept of a filter that will analyze and display individual spectral components of a two-dimensional image

[a]Author to whom correspondence should be addressed; electronic mail: pritish@chuma1.cas.usf.edu
[b]Currently at: E-Tek Dynamics, 1865 Lundy Avenue, San Jose, CA 95131.

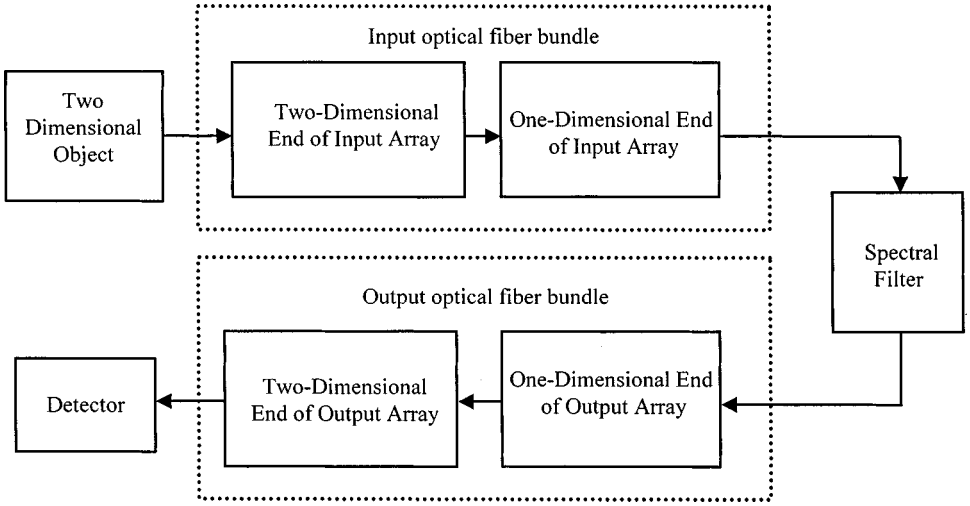

FIG. 1. Block diagram of the continuously tunable two-dimensional spectral filter.

(henceforth referred to as the ''object'') in real time is illustrated in the block diagram in Fig. 1. It can be constructed by performing the sequence of procedures outlined below.

Step 1: Suitably imaging the two-dimensional multicolor object on a two-dimensional array of optical fibers.

The two-dimensional image may either be (a) directly imaged without magnification on to a two-dimensional array of optical fibers or (b) magnified (for higher spatial resolution imaging) or reduced (for greater field-of-view imaging) prior to incidence on the two-dimensional array. The purpose of the two-dimensional array is to digitize the optical image. The spatial resolution of the ultimate spectral image depends on the resolution of the digitization. The diameter of each individual fiber as well as the density of the two-dimensional packing determines the resolution of the digitization. The use of presently available 10 μm single-mode fibers with possible interfiber spacings less than 20 μm including cladding can easily provide high spatial resolution. The combination of available fiber diameters and magnification of the image prior to incidence on the two-dimensional array allows spatial resolutions of a micron or better, if needed.

Given a fiber diameter, the arrangement of the two-dimensional fiber array depends upon the application. For example, a close-packed arrangement may be used for greatest resolution while a scattered sparse arrangement may suffice for site-specific multipoint imaging.

Step 2: Reshaping the output of the two-dimensional fiber array into a linear array.

The other ends of the fiber constituting the two-dimensional input array are shaped into a linear array to provide a linear image for subsequent spectral filtering. It is advantageous (especially in a densely packed two-dimensional array) to arrange the linear array in such a way that adjacent fibers in the linear array are connected at the two-dimensional end to spatially contiguous regions. This kind of sequencing of the fibers in the one-dimensional array reduces errors in spatial fidelity in the ultimately obtained spectral image.

Step 3: Spectrally filtering the resultant linear digitized image to obtain the desired spectral component of the image.

The optical image of the one-dimensional input fiber array is then used as the object for a spectral filter (such as a monochromator) to disperse its constituent spectral components. A desirable configuration is to image the one-dimensional input image 1:1 at the output of the monochromator. The narrow width of the input array (which constitutes, in effect, the width of the input slit to the monochromator), coupled with the achievable spectral dispersion of typical triple grating monochromators permits angstrom level resolution of the output spectral image.

An identical one-dimensional fiber array constitutes the output slit of the monochromator. Simply by adjusting the grating of the monochromator the desired spectral component of the linear image can be obtained on the output one-dimensional array. The process of this tunable spectral filtering thus analyzes the input light into its spectral components and permits the selection of any desired individual frequency component of the initial multicolor image while maintaining the spatial integrity of the linear input image.

Step 4: Imaging the filtered linear output on a second linear fiber optic array.

By imaging the output of the spectral filtering on to an identical one-dimensional fiber array there is a one-to-one correlation between the spatial information contained in the two linear arrays. The light from each fiber in the input array to the monochromator is filtered and the results of the filtration obtained at the corresponding spatial counterpart at the output array.

Step 5: Reconstructing the desired two-dimensional monochromatic spectral image by reshaping the output of the second fiber bundle into a two-dimensional array.

The light at the spatial location of each fiber of the output linear array can be traced back to its corresponding origin in the initial two-dimensional array (prior to spectral filtering). Therefore, the other ends of the fibers constituting the output linear array can be reconstituted into the same configuration as the original two-dimensional array to obtain the spectrally filtered two-dimensional image of the original object at any desired wavelength.

Step 6: Detecting the two-dimensional spectral image.

The final image can be detected using a camera (such as a CCD camera) and then displayed real time on a video monitor. There are two possible modes of detection.

(a) If the original object is a dynamically evolving entity

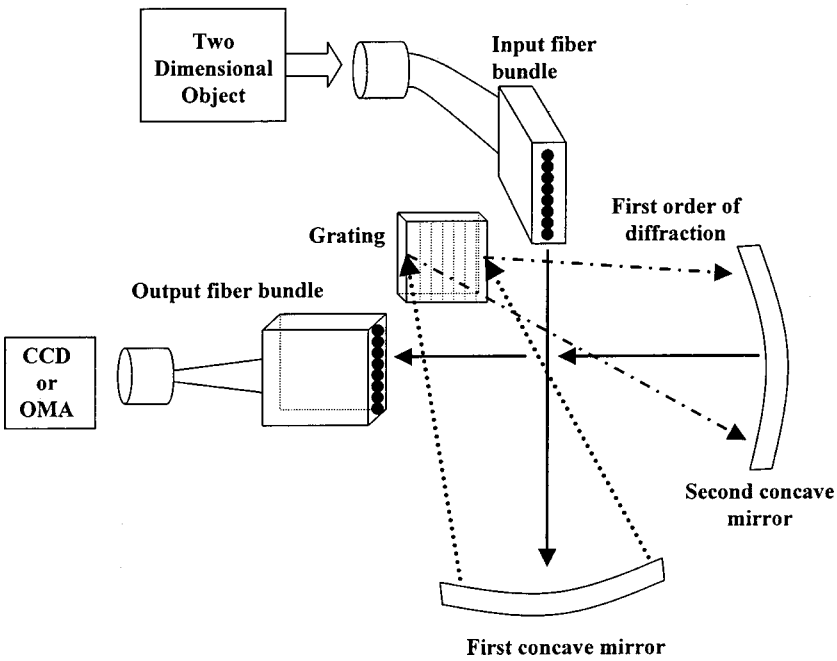

FIG. 2. Optical arrangement of the prototypical filter system.

(such as the fluorescence from an expanding laser-ablated plume), a fast time-gated camera (such as an CCD camera) can be used to capture transient two-dimensional spectral images. Currently, commercially available gate widths for such cameras permit attainable temporal resolutions for such dynamic images in the 10 ns time scale.

(b) The other mode of detection is time-integrated detection of images where the dynamic characteristics are not required. No fast gating is required for this mode, which is particularly suitable for objects exhibiting extremely low light intensities.

III. PROTOTYPICAL IMPLEMENTATION OF THE TWO-DIMENSIONAL SPECTRAL FILTRATION

A prototype of the proposed two-dimensional optical filter was constructed to investigate the feasibility and performance of this technique. The optical arrangement is schematically illustrated in Fig. 2.

As shown in Fig. 2, the two-dimensional object is incident on the input two-dimensional array so that the object is digitized into many pixels. The light in each pixel propagates inside each individual fiber and scatters out from the one-dimensional end of the fiber bundle. The construction of the two-dimensional to one-dimensional fiber array is discussed later in detail. This scattered light is collected by the first concave mirror, and sent to the grating as a collimated parallel beam. The first order diffraction from the grating is incident on the second concave mirror. The image of the input one-dimensional array is formed in the focal plane 12 in. away from the second concave mirror, and it constitutes a ribbon of color consisting of a series of horizontal color lines. In each horizontal line, representing the image of a single pixel, the color varies from blue to red from one end to the other. Each color line in the color ribbon is therefore the image of a corresponding fiber in the one-dimensional end of the input fiber bundle. The one-dimensional fiber array of the output fiber bundle is vertically aligned on the desired spectral region of the band so that it can collect light from the corresponding fibers in the input one-dimensional array. The image is finally restored back to its two-dimensional form through the two-dimensional array of the output fiber bundle. After the output fiber bundle, either a gated CCD camera or optical multichannel analyzer (OMA) system, as necessary for the specific experiment, is used to detect the filtered image.

A. Fiber arrays and their fabrication

The two fiber bundles used in our prototype need to be identical. One end of each fiber bundle had a two-dimensional 10×10 fiber array tapering off to a 100 fiber element one-dimensional array at the other end of the bundle (Fig. 3). The silica fibers had a 200 μm core diameter and a 240 μm total diameter including the cladding. The total length of the one-dimensional array was 24 mm, and the individual fiber lengths for each fiber bundle were 40 cm. The transmission range for the fibers used spans the visible and infrared region of the spectrum from 400 to 1200 nm. Either of these two fiber bundles could be used as the input or output fiber bundle. The ends of all the fiber bundles were polished to a surface roughness better than 1 μm.

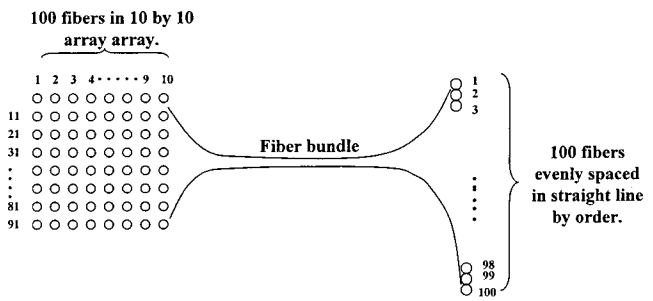

FIG. 3. Spatial arrangement of the fiber array in a bundle. The input and output bundles are identical.

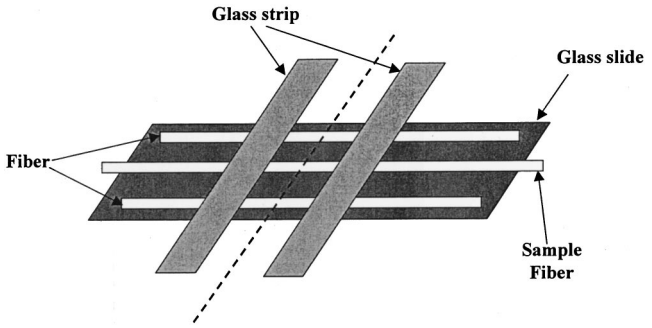

FIG. 4. One-fiber-high channel constructed to permit fabrication of the one-dimensional arrays of the fiber bundles.

Since the input one-dimensional array was imaged with unit magnification exactly on to the output one-dimensional array, it was crucial that the two one-dimensional arrays have exactly the same spatial structure including the same microarrangement and spacing of each individual fiber end. Otherwise, a fiber in the output one-dimensional end would not be able to collect the light from its corresponding counterpart in the input one-dimensional fiber array or not be able to collect light at the desired wavelength.

The two fiber bundles were fabricated from 100 fibers, each fiber being 80 cm in length. The most important part during the fabrication was to make the two one-dimensional arrays exactly the same. Two fibers were glued parallel to each other onto a glass slide. Another two small glass pieces were glued on top of the fibers. This created a narrow slot to hold fibers in a one-dimensional array (Fig. 4). The 100 fibers were inserted into the slot one by one next to each other, and the fibers and glass slide were glued together with epoxy. After the glue was completely dry, the whole piece was cut apart along the dotted line (Fig. 4) using a diamond saw. Finally, both cut ends of each fiber bundle were mechanically polished to complete the fabrication of the two identical one-dimensional arrays.

For the fibers in the two-dimensional array, fiber holders were designed to hold the fibers. One hundred holes were drilled in a 10×10 square array (shown in Fig. 3) in two plastic disks each of which was $\frac{1}{4}$ in. thick and 24 mm in diameter. Each hole had a diameter of 508 μm, and the center-to-center distance between two consecutive holes was 2 mm. Next, 200 hypodermic needles were inserted into these 200 holes on the two disks. It was ensured that all the needles were inserted from one side of each disk, and reached the surface on the other side of the disk. Each needle was 1.375 in. long with 250 μm inner diameter and was glued perpendicular to the disk by epoxy. These long needles provided better support to the fibers, as well as providing holes of the right size to position the fibers. The third step was to fit the disks inside glass tubes of the same inner diameter and attach them together with epoxy. Last, the fibers were inserted into the needles, using a flat microslide pushing against all the fiber ends to ensure that all the fiber ends were in the same plane. The fibers were finally fixed in position by mounting wax to form the two-dimensional array of the fiber bundle.

B. Optical configuration of the prototype

The monochromator, in our prototype, consisted of a single square plane reflection grating 1 in.$\times$1 in. in size, with 1200 grooves per mm. It was mounted on a stage so that the grooves on the grating were vertically positioned (Fig. 2). The stage provided freedom of movement in three dimensions, one for horizontal adjustment, one for vertical adjustment, and one for rotation along a vertical axis. Though having the maximum intensity, the zeroth order of diffraction from the grating is not usable as there is no angular separation between the spectral components of the image. Only the first order diffraction was collected by the concave mirror.

The two mirrors were front reflection concave mirrors. The mirror diameter was 6 in. with a focal length of 12 in. The advantage of choosing a mirror instead of a lens-based system was to eliminate chromatic aberration. The first concave mirror was positioned 12 in. away from the one-dimensional end of the input fiber bundle while the other concave mirror was similarly placed 12 in. away from the one-dimensional end of the output fiber bundle, so that the two mirrors in effect form a telescope of unit magnification. This arrangement ensured that the beams incident onto the grating were parallel beams and allowed accurate one-to-one imaging between the input and output one-dimensional arrays. The spectrum from the grating therefore avoided inter-fiber spatial and spectral overlap, thereby ensuring the smallest bandwidth and lowest crosstalk for our filter system.

IV. CHARACTERIZATION OF THE PERFORMANCE OF THE TWO-DIMENSIONAL SPECTRAL IMAGER

A. Performance characterization using coherent monochromatic radiation

The filter system was characterized using two kinds of light sources. The He–Ne laser was used first, because of its monochromaticity and directionality that allowed ease of alignment and calibration. A series of experiments were performed to assess a variety of characteristics of the fabricated two-dimensional spectral imaging system.

1. One-to-one correspondence of the fiber array

The first figure of merit was to verify the one-to-one correspondence between each fiber in the two-dimensional input array and its counterpart in the two-dimensional output array. The two-dimensional input fibers were all illuminated by light from a He–Ne laser at 632.8 nm while the output image from the two-dimensional output fibers was monitored using a CCD camera. During this procedure, the He–Ne beam was expanded with a lens to allow coverage of all the fibers in the input two-dimensional array. The CCD image of the two-dimensional output is shown in Fig. 5. The tilt of the 10×10 array in the image is due to a tilt in the orientation of the CCD camera. The variations in the spatial intensity profile at each fiber output in the CCD image are due to variations in the intensity of the He–Ne laser on the input two-dimensional fiber array. There were a few misalignments in

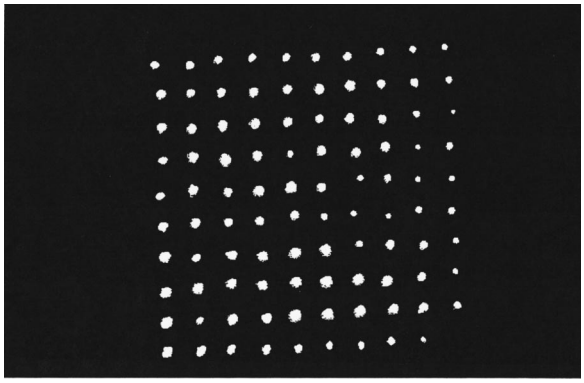

FIG. 5. Output image of the filter system for He–Ne laser illumination of all the fibers of the two-dimensional input array. The last fiber at the lower right corner (the 100th fiber) was accidentally broken during fabrication and thus exhibited no output. Such defects can easily be avoided in commercial fabrication of these arrays.

the two-dimensional output array of our prototype, noticeably for fiber numbers 57, 68, and 77. This was due to mispositioning of the hypodermic needles and had no effect on the subsequent proof-of-principle data. It is important to emphasize that the two one-dimensional arrays were exactly identical and the light from the input two-dimensional array was accurately routed to its counterpart in the output two-dimensional array. The significant observation is that all the fibers in the output array were illuminated on tuning the grating to the proper position for the He–Ne wavelength. Even a slight detuning extinguished the illumination completely.

2. Investigation of crosstalk between fibers

An issue of concern is the spatial integrity of the two-dimensional image after transmission through the filter. For example, if the image of each input one-dimensional fiber is much bigger than the actual size of the output one-dimensional fiber (as shown in Fig. 6), it is possible for the light from one input fiber to go into other uncorresponding fibers. This phenomena is referred to as spatial crosstalk. Such spatial crosstalk, if it exists, could manifest itself in spatial as well as spectral diffusion and resultant distortion of the transmitted image.

Because of the structure of the fiber array (Fig. 3), at the output end of the fiber bundle, the first fiber to the tenth fiber

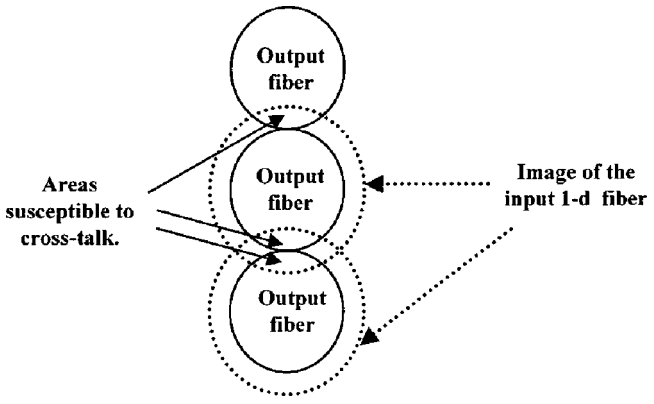

FIG. 6. Diagrammatic representation of the possible origin of crosstalk.

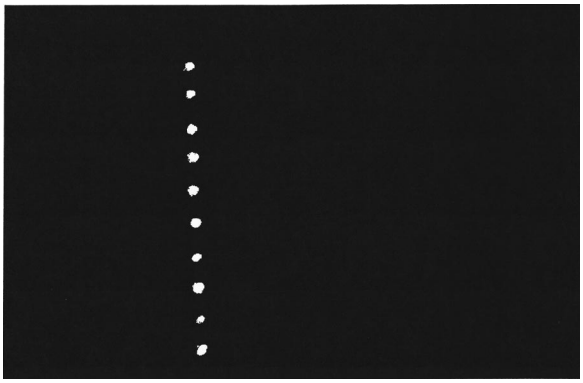

FIG. 7. Crosstalk check for column 2. The ten fibers, from top to bottom, are number 2–92. No fibers on either side were observed to be illuminated.

are successively horizontally adjacent to each other, the 11th to the 20th fiber are horizontally adjacent, and so on. We checked the crosstalk column by column for each of the ten columns. An example of such a check is illustrated in Fig. 7 for which only the second column, i.e., the ten input fibers numbered 2,12,22,...,92 in Fig. 3 were exclusively illuminated. For the image of each fiber in this column, there was no illumination of adjacent columns on either side in the output image on the CCD detector. Each column, from column 1 to column 10, exhibited the same lack of crosstalk. Similar results were obtained on checking the illumination of isolated horizontal rows. These results are particularly significant because adjacent fibers in the one-dimensional array were placed in direct contact with each other, as discussed in a description of the fabrication process in Sec. III A.

3. Pattern recognition

In this filter system, the two-dimensional object is effectively digitized into pixels and rearranged into a one-dimensional image. Therefore, the system must eventually have the ability to restore the two-dimensional image accurately. Different shapes for input illumination were used to check the ability of shape restoration of the filter system. Figure 8 shows the results for a variety of input spatial patterns. The results show the pattern restoration ability of the filter system as well as the spatial movements of the output image corresponding to movements of the input object. The low spatial resolution of the two-dimensional images is caused by the sparseness of the input array in our prototype. Since the purpose of these experiments was to illustrate proof of principle, a limited number of fibers were used in the two-dimensional array. These fibers were separated by a 2 mm center-to-center distance between every two fibers and this spacing determined the low resolution of the resultant image. This can be easily improved in a commercial system by arranging fibers in contact with each other, similar to the array for a CCD detector.

4. Efficiency of the prototypical filter

We used an OMA, tuned to the 632.8 nm wavelength of the He–Ne laser, to measure the throughput efficiency of the filter system. The output efficiency was measured by comparing the OMA signals at the input and output of the filter

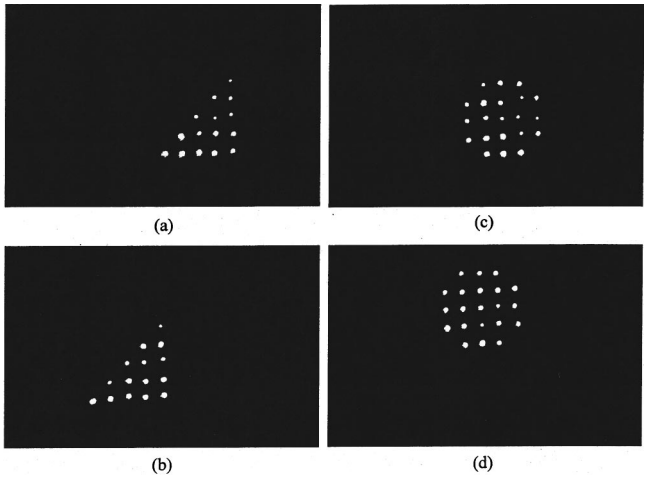

FIG. 8. Output images when the input objects were a triangle and a circle. (a) The filter output when the input was a triangle. (b) The image when the triangle was moved down and to the left side. (c) The filter output when the input was a circle. (d) The image when the circle was moved up and to the left.

system. The fiber detector for the OMA was covered by a 310 μm diameter pinhole. The He–Ne spectral line was detected using the OMA at the input end of the fiber bundle with a 3.3 neutral-density (ND) filter, and recorded a peak reading of 304 609 counts [Fig. 9(a)]. At the final output end of the filter system, the OMA showed a peak intensity reading of 91 454 counts [Fig. 9(c)] with a ND filter of 2.9. The output efficiency (e), defined as the ratio of output intensity to the input intensity, is therefore given by

$$e=\frac{91\,454}{304\,609}\times\frac{10^{-3.3}}{10^{-2.9}}\times\left(\frac{310}{200}\right)^2=0.287=29\%. \quad (1)$$

The above calculation corrects for the difference between the core diameter of the fiber and the diameter of the pinhole covering the fiber connected to the OMA. This indicates a net loss of 71% of the light in going through our system. Of this 71% loss, 9% was lost at the output of the first fiber bundle. At the end of the first fiber bundle, the peak output intensity was recorded to be 115 314 counts [Fig. 9(b)], which is 90.95% of the input intensity. The internal transmission loss of the fiber itself is less than 1% especially for our fiber length of less than a meter. The rest of the ~8% loss can be attributed to increased reflectivity at the two-dimensional input array due to the inadequacy of our mechanical polishing combined with non-normal incidence of light onto the input two-dimensional array.

Beyond the first fiber bundle, the efficiency based on the spectra shown in Figs. 9(b) and 9(c) is calculated to be

$$e'=\frac{91\,454}{115\,314}\times\frac{10^{-3.3}}{10^{-2.9}}=0.32=32\%. \quad (2)$$

This includes the net throughput of the dispersion and imaging system in the filter as well as the final output optical fiber bundle.

These initial results have not been optimized to maximize the net efficiency of the system. The imaging system was constructed using components currently available in the laboratory. For example, the light output of the first one-dimensional fiber bundle incident onto the concave mirror has an oval shape with an approximate spot size of 3 cm by 4 cm. The concave mirror reflects the light in a parallel beam to the grating, with a circular spot size approximately 4 cm in diameter. If the size of the grating is increased to 5 cm $\times$5 cm instead of only 2.5 cm$\times$2.5 cm, it would be able to collect light more efficiently from the concave mirror, and therefore improve the efficiency by a factor of 2.

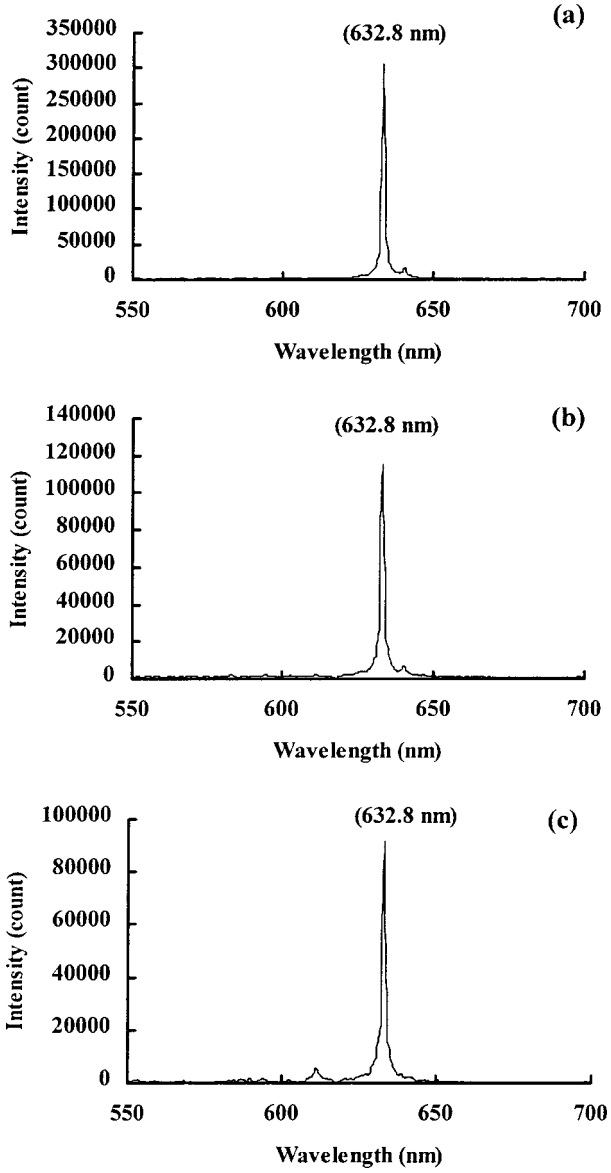

FIG. 9. Intensity of He–Ne laser at different positions of the filter system. (a) Laser intensity at the input with a 3.3 ND filter. (b) Laser intensity at the one-dimensional output of the input fiber bundle, with a 3.3 ND filter. (c) Final laser intensity at the two-dimensional output of the filter system with a 2.9 ND filter.

B. Characterization using broadband illumination

As opposed to the monochromatic emission of the He–Ne laser, a xenon arc lamp provides broadband light covering a wide wavelength range, from 50 to 1500 nm. It is therefore an ideal light source to calibrate the spectral response of our filter system.

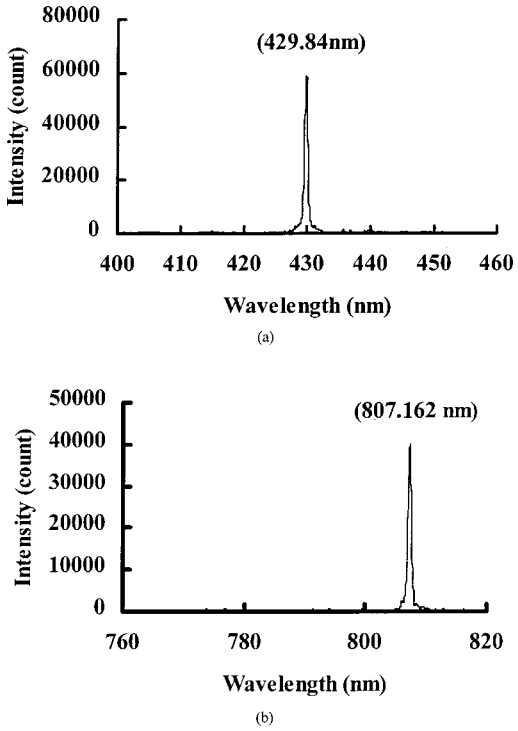

FIG. 10. Two examples demonstrating the range of wavelengths that the system can filter. (a) A representative spectrum in the short wavelength range. (b) A representative spectrum in the long wavelength range.

1. Investigation of spectral tunability

The wavelength range over which the filter is continuously tunable was tested by using the OMA system. A xenon arc lamp was used to illuminate the input two-dimensional array while the fiber detector of the OMA system was placed adjacent to a desired fiber of the output two-dimensional array (Fig. 2). Simple angle tuning of the grating allowed output frequency selectivity of the two-dimensional image. Figure 10 demonstrates two examples of this continuous tunability spanning the range from 430 nm (the blue) to a wavelength of 807 nm (beyond the visible spectrum). Therefore, the filter range is limited only by the wavelength that the fiber can transmit. The transmission range of the fiber used is from 400 to 1200 nm, which determines the ultimate functional range of our silica-based filter system.

2. Frequency selectivity of the spectral filter

When the filter system is tuned to a specific wavelength, other wavelengths should be efficiently rejected in the output. This lack of ''spectral leakage'' is demonstrated in Fig. 11. When the filter was tuned to a wavelength in the green region of the visible spectrum ($\lambda = 550$ nm) a broad wavelength scan from 400 to 700 nm, covering the majority of the visible spectrum, showed no evidence of emission at any other wavelengths. This was verified at other transmission wavelengths as well and there was no observable spectral leakage in our filter system.

3. Bandwidth of the spectral filter

The transmitted bandwidth can be obtained by high resolution measurements of any spectral line detected by the

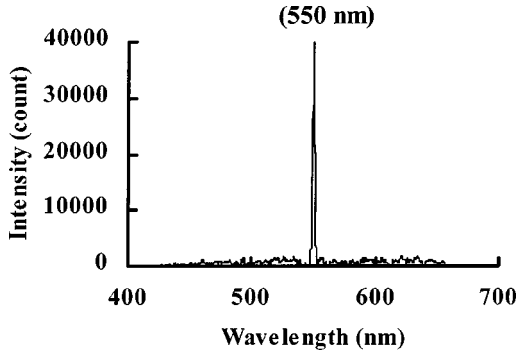

FIG. 11. Typical output spectrum during the broad wavelength range scans to check for spectral leakage.

OMA. Figure 12 shows the bandwidth of the spectra depicted in Fig. 10. The bandwidths (full width at half maximum) for both short and long wavelength ranges are around 0.6 nm, which indicates a very uniform bandwidth throughout the tunable range. The theoretical bandwidth, on the basis of the resolution of our diffraction grating and the diameter and position of the fibers used in the one-dimensional output array, is calculated to be 0.66 nm, which is consistent with our experimentally observed values. This calculated value for bandwidth is obtained by considering the ratio of the spatial spread of the wavelength range in the plane of the band to the core diameter of the output one-dimensional fiber. A factor of 2 was used to compensate for the finite size of the one-dimensional input fiber.

4. Measurement of uniformity of spectral transmission along the fiber array

If the position of a fiber in any of the one-dimensional arrays is off slightly relative to other fibers, the wavelength

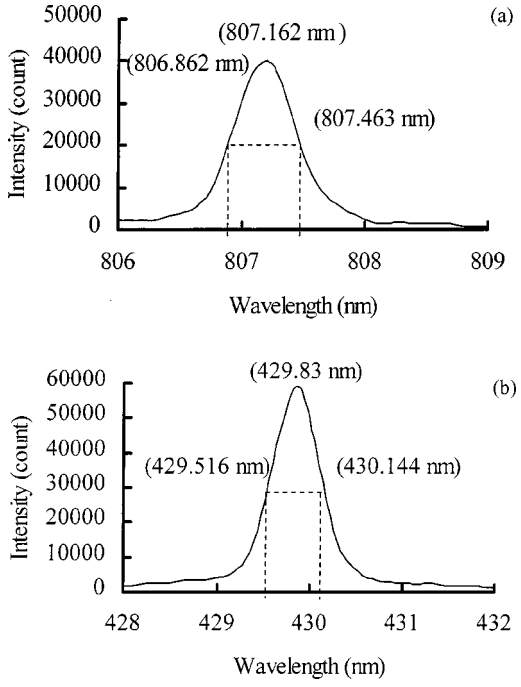

FIG. 12. Measurement of bandwidth for the filter system. Each pixel was 0.08 nm. (a) The measured bandwidth at the long wavelength range is 0.601 nm. (b) The measured bandwidth at the short wavelength range is 0.628 nm.

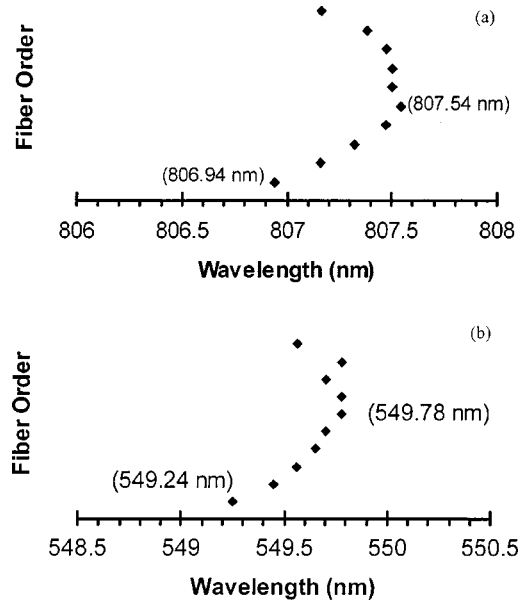

FIG. 13. Spectrum uniformity test using fibers in column five. (a) Spectrum uniformity tested around a wavelength of 807.25 nm. (b) Spectrum uniformity tested around a wavelength of 549.5 nm.

selected will be different from that expected. We used the OMA to test fibers in column 5 for spectral uniformity along the fiber array. By choosing fibers in a column we ensure sampling of fibers that are evenly spaced in the one-dimensional array (refer to Fig. 3). Further, sampling any entire column affords data over a large range of the one-dimensional array and is thus truly representative of the maximum extent of the spectral nonuniformity. The wavelength of the peak value from each fiber was recorded fiber by fiber. These wavelengths are plotted in Fig. 13 and showed a curvature. The largest deviation in wavelength throughout the entire range is 0.6 and 0.54 nm for Figs. 13(a) and 13(b), respectively. This maximum variation is however within the 0.6 nm bandwidth discussed in the previous subsection and is therefore not a significant problem. Similar results were obtained for fibers in other columns. This confirms the high accuracy in positioning down the one-dimensional array in our prototype.

The observed curvature is due to off-axis reflections from the concave mirror. If the system filters a single frequency light source, such as the output of a He–Ne laser (632.8 nm), the images of the first one-dimensional array fibers have a slight spatial curvature introduced by the off-axis fibers. As a result, the second one-dimensional array of fibers will pick up slightly disparate wavelengths in a multiwavelength spectrum. Interestingly, from Fig. 13, the positions of the points are not random; they tend to form a smooth curve. This provides a remedy for alleviating this slight problem of spectral nonuniformity. The solution is to match the spatial arrangement of the second one-dimensional array according to the curvature of the imaging mirror, so that all the fibers can image the exact wavelength selected, thereby resulting in better spectral uniformity.

5. Spectral signature-based pattern recognition

An essential function of the filter system is to allow spatial patterns of a selected wavelength to pass through. In order to test this function, two object images were projected onto the input of the filter system simultaneously. One of these objects was a triangle at a wavelength of 450 nm, while the other one was rectangular at a wavelength of 458 nm. The wavelengths were generated using an Ar laser (458 nm) and a Xe arc lamp with a commercial filter at 450 nm. By appropriately tuning the angle of the grating, only the desired pattern can be selected at the output of the filter system and recorded by a CCD camera (Fig. 14). There is no observable interference between the images at these two different but closely spaced wavelengths. In both cases, the output of the filtration system was identical to the shape and size of the corresponding spectral component in the dual-wavelength input object.

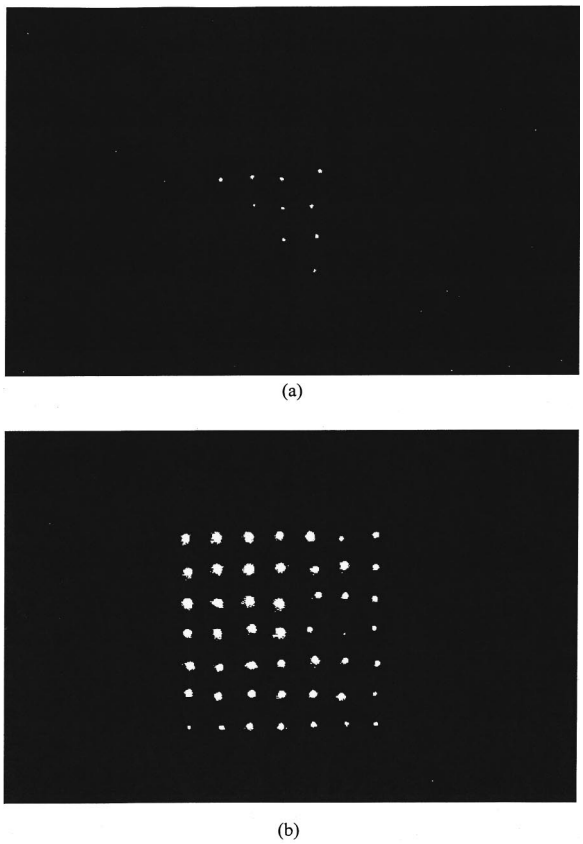

FIG. 14. Pattern recognition based on spectral signatures. (a) The output was a triangle when the wavelength of 450 nm was selected. (b) The output was rectangular when a wavelength of 458 nm was selected.

V. DISCUSSION

The presented characterization of the performance of our laboratory prototype confirms the possibility of implementation of the two-dimensional spectral filtering concept introduced in this article. Commercially fabricated fiber arrays with more precise positioning and better end-polishing coupled with optimized light collection and dispersion of the input light by a larger grating should lead to enhanced efficiency. This will permit the analysis of a two-dimensional multiwavelength object into its spectral constituents with a potential wavelength resolution on the order of angstroms and micron (or better) spatial resolution. Gated viewing can provide the derivation of constituent monochromatic two-

dimensional images with temporal resolution of dynamic events on the 10 ns timescale. The proposed two-dimensional spectral imager is continuously tunable and any wavelength that can be transmitted by the optical fibers and dispersed by the monochromator will be available for viewing. Using 10μm diameter fibers, a 50×50 two-dimensional array resulting in a one-dimensional array 25 mm in length is practically feasible. Larger arrays are also possible by correcting for off-axis aberrations in the correspondingly larger linear arrays. Repositioning of the elements of the linear array to counteract systematic spherical aberrations is possible based on the observation of trends such as those in Fig. 13.

There are numerous applications for this imager in the viewing of two-dimensional objects, in which the ability to view the different spectral components while maintaining spatial integrity is important. For example, CCD imaging has been used in the imaging of laser-ablated plume dynamics by viewing the plume fluorescence.[53–56] Our proposed filter is particularly suitable for studying plume emission during the laser ablation process for the growth of thin films. We are currently exploring the use of the imager demonstrated in this article to provide species-resolved dynamic information about the spatial expansion and propagation of individual atomic and molecular species in a multicomponent laser-ablated plume. This should be possible as the demonstrated resolution and tunability of the spectral imager allows the isolation of emission from any atomic or molecular species and two-dimensional display in real time.

Other potential applications include, but are not limited to, plasma diagnostics, combustion diagnostics (such as rocket plume imaging), real time process monitoring for fluorescent processes, medical imaging (for example, the fluorescent detection of cancer cells), and sensing of spatial temperature variations (via blackbody radiation detection using a suitable fiber material).

ACKNOWLEDGMENTS

This research was supported in part by the National Science Foundation (Grant No. DMI-9622114 and Grant No. DMI-9978738) and the United States Department of Energy (Grant No. DE-FG02-96ER12199). The technical assistance of J. B. Cuff is acknowledged.

[1] G. Kopp and M. Derks, Photonics Spectra **31**, 125 (1997).
[2] N. D. Finkelstein, W. R. Lempert, and R. B. Miles, Opt. Lett. **22**, 537 (1997).
[3] J. Sabbaghzadeh, W. Buell, J. Holder, and M. Fink, Appl. Phys. B: Lasers Opt. **60**, S261 (1995).
[4] Z. Y. Liu, I. Matsui, and N. Sugimoto, Opt. Eng. **38**, 1661 (1999).
[5] A. P. Yalin and R. B. Miles, Opt. Lett. **24**, 590 (1999).
[6] P. Golz and P. Andresen, Appl. Opt. **35**, 6054 (1996).
[7] M. H. Duan, Y. M. Li, J. X. Tang, and Q. J. Wang, Acta Phys. Sin. (Overseas Ed.) **4**, 33 (1995).
[8] N. D. Hung, Y. Segawa, Y. H. Meyer, P. Long, and L. H. Lai, Appl. Phys. B: Lasers Opt. **62**, 449 (1996).
[9] A. N. Naumov, R. B. Miles, P. Barker, and A. M. Zheltikov, Laser Phys. **10**, 622 (2000).
[10] M. Jablonski, Y. Takushima, K. Kikuchi, Y. Tanaka, K. Furuki, K. Sato, and N. Higashi, Electron. Lett. **36**, 1139 (2000).
[11] A. Ankiewicz and G. D. Peng, Electron. Lett. **33**, 2151 (1997).
[12] Y. A. Nestrizhenko, Opt. Spectrosk. **65**, 210 (1988).
[13] S. Tibuleac, P. P. Young, R. Magnusson, and T. R. Holzheimer, IEEE Microwave Guid. Wave Lett. **9**, 19 (1999).
[14] A. Safaaijazi and C. C. Chang, IEEE J. Quantum Electron. **32**, 1063 (1996).
[15] A. Inoue, T. Iwashima, T. Enomoto, S. Ishikawa, and H. Kanamori, IEICE Trans. Electron. **E81C**, 1209 (1998).
[16] C. J. Chung and A. Safaaijazi, J. Lightwave Technol. **10**, 42 (1992).
[17] A. Safaaijazi and J. C. Mckeeman, J. Lightwave Technol. **9**, 959 (1991).
[18] N. S. Gluck and W. J. Gunning, Appl. Opt. **28**, 5110 (1989).
[19] J. Jagannathan and A. Safaaijazi A, J. Mod. Opt. **44**, 581 (1997).
[20] C. H. Lee, S. S. Lee, H. K. Kim, and J. H. Han, IEEE Photonics Technol. Lett. **8**, 1725 (1996).
[21] M. Tschanz, A. Rebane, and U. P. Wild, Opt. Eng. **34**, 1936 (1995).
[22] S. C. Chao and M. S. Wu, J. Low Temp. Phys. **12**, 1777 (1994).
[23] G. Kopp, Proc. SPIE **2873**, 324 (1997).
[24] R. Y. Tsai, S. C. Shiau, D. Lin, F. C. Ho, and M. Y. Hua, Appl. Opt. **38**, 5452 (1999).
[25] J. H. Kim, Opt. Eng. **37**, 3031 (1998).
[26] M. J. Vrhel, H. J. Trussell, and J. Bosch, J. Electron. Imaging **4**, 6 (1995).
[27] Q. G. Li and H. G. Li, Appl. Opt. **24**, 1180 (1985).
[28] A. Jun-Won, K. Jung-Hoi, K. Nam, and L. Kwon-Yee, in *Conference on Lasers and Eletro-Optics*, Vol. 4, 1999 OSA Technical Digest Series (Optical Society of America, Washington, DC, 1999), p. 819.
[29] G. A. Rakuljic and V. Leyva, Opt. Lett. **18**, 459 (1993).
[30] M. Yoshikawa and K. Kameda, IEICE Trans. Electron. **E77C**, 1526 (1994).
[31] D. E. Battey, J. B. Slater, R. Wludyka, H. Owen, D. M. Pallister, and M. D. Morris, Appl. Spectrosc. **47**, 1913 (1993).
[32] Z. Q. Wang, C. M. Cartwright, C. Soutar, and W. A. Gillespie, Appl. Opt. **32**, 715 (1993).
[33] G. A. Rakuljic and V. Leyva, Opt. Lett. **18**, 459 (1993).
[34] M. J. Pelletier and R. C. Reeder, Appl. Spectrosc. **45**, 765 (1991).
[35] K. A. Christensen, N. L. Bradley, M. D. Morris, and R. V. Morrison, Appl. Spectrosc. **49**, 1120 (1995).
[36] R. S. Weis and T. K. Gaylord, J. Opt. Soc. Am. A **5**, 1565 (1988).
[37] D. M. Rust, Opt. Eng. **33**, 3342 (1994).
[38] W. Gunning, J. Pasko, and J. Tracy, Proc. Soc. Photo-Opt. Instrum. Eng. **268**, 198 (1981).
[39] M. Y. Liu and S. Y. Chou, Appl. Phys. Lett. **68**, 170 (1996).
[40] H. Wright, C. M. Crandall, and P. Miller, Laser Focus World **32**, 85 (1996).
[41] Y. A. Nestrizhenko, Opt. Spectrosk. **74**, 410 (1993).
[42] W. Q. Zhang, Optik (Stuttgart) **111**, 85 (2000).
[43] T. W. Tukker, C. Otto, and J. Greve, J. Opt. Soc. Am. B **16**, 90 (1999).
[44] J. S. Wang, G. X. Ai, G. F. Song, B. Zhang, X. M. Ye, Y. P. Nie, T. Chiveh, W. Tsay, and H. S. Li, Sol. Phys. **161**, 229 (1995).
[45] K. Naganuma, G. Lenz, and E. P. Ippen, IEEE J. Quantum Electron. **28**, 2142 (1992).
[46] S. D. Zhu, Appl. Opt. **29**, 410 (1990).
[47] J. Staromlynska, S. M. Rees, and M. P. Gillyon, Appl. Opt. **37**, 1081 (1998).
[48] R. S. Seymour, S. M. Rees, J. Staromlynska, J. Richards, and P. Wilson, Opt. Eng. **33**, 915 (1994).
[49] A. L. Aleksandrovskii, T. A. Vinogradova, N. P. Depman, and V. V. Tarasenko, Sov. J. Opt. Technol. **59**, 216 (1992).
[50] E. J. Rhodes, *Applications of the Magneto-Optical Filter to Stellar Pulsation Measurements* (National Aeronautics and Space Administration, Washington DC, 1985).
[51] D. M. Rust, *Continued Development of an Ultra-Narrow Bandpass Filter for Solar Research* (National Aeronautics and Space Administration, Washington DC, 1993).
[52] H. A. Macleod, *Thin-Film Optical Filter* (Macmillan, New York, 1986).
[53] D. B. Geohegan, Appl. Phys. Lett. **60**, 2732 (1992).
[54] D. B. Geohegan, Appl. Phys. Lett. **62**, 1463 (1993).
[55] D. B. Geohegan, Mater. Res. Soc. Symp. Proc. **285**, 27 (1993).
[56] P. Mukherjee, S. Chen, and S. Witanachchi, Appl. Phys. Lett. **74**, 1546 (1999).